

Growth and physical properties of epitaxial metastable cubic TaN(001)

C.-S. Shin, D. Gall, P. Desjardins, A. Vailionis, H. Kim, I. Petrov, and J. E. Greene^{a)}

Department of Materials Science, the Materials Research Laboratory, and the Coordinated Science Laboratory, University of Illinois, Urbana, Illinois 61801

M. Odén

Department of Mechanical Engineering, Linköping University, S-581 83 Linköping, Sweden

(Received 14 July 1999; accepted for publication 22 October 1999)

We report the growth of epitaxial metastable B1 NaCl structure TaN(001) layers. The films were grown on MgO(001) at 600 °C by ultrahigh vacuum reactive magnetron sputter deposition in mixed Ar/N₂ discharges maintained at 20 mTorr (2.67 Pa). X-ray diffraction and transmission electron microscopy results establish the epitaxial relationship as cube-on-cube, (001)_{TaN}||(001)_{MgO} with [100]_{TaN}||[100]_{MgO}, while Rutherford backscattering spectroscopy shows that the layers are overstoichiometric with N/Ta=1.22±0.02. The room-temperature resistivity is 225 $\mu\Omega$ cm with a small negative temperature dependence between 20 and 400 K. The hardness and elastic modulus, as determined by nanoindentation measurements, are 30.8±0.9 and 457±16 GPa, respectively.

© 1999 American Institute of Physics. [S0003-6951(99)04450-2]

Polycrystalline TaN_x thin films are presently used in a variety of applications including hard wear-resistant coatings on tools, diffusion barriers in integrated circuits, resistors, and mask layers for x-ray lithography. Unlike the more common hard-coating material, the IVB–VA compound TiN, little is known about the fundamental properties of cubic TaN, a metastable VB–VA compound. While the Ti–N equilibrium phase diagram is relatively simple with the only compounds being tetragonal Ti₂N and NaCl-structure TiN, the Ta–N system is extremely rich.^{1,2} In addition to the equilibrium phases bcc Ta, solid-solution α -Ta(N), hcp- γ -Ta₂N, and hexagonal ϵ -TaN, a variety of metastable phases have been reported. These include tetragonal β -Ta, bcc β -Ta(N), hexagonal WC structure θ -TaN, cubic B1 NaCl structure δ -TaN, hexagonal Ta₅N₆, tetragonal Ta₄N₅, and tetragonal Ta₃N₅.^{1,2} This complexity makes it challenging to grow phase-pure TaN_x compounds and, hence, little is known about fundamental properties of these materials. There are no reports on single-crystal TaN_x layers.

We expect that cubic TaN, like TiN³ and NbN⁴ which have the same NaCl crystal structure, will have a wide single-phase field and can support large vacancies concentrations on both cation and anion sublattices. In the case of TiN, N/Ti can vary from 0.6 to \approx 1.2 (Ref. 3).

In this letter, we present evidence for the growth of epitaxial single-crystal TaN thin films on MgO(001). X-ray diffraction (XRD) and transmission electron microscopy (TEM) indicate that the alloys are single-phase B1 NaCl structure TaN with a room-temperature resistivity of 225 $\mu\Omega$ cm. Nanoindentation measurements show that the elastic modulus of the TaN films is comparable to that of TiN while the hardness is more than 50% higher.

All TaN_x films, 0.5 μm thick, were grown in a load-locked multichamber ultrahigh vacuum (UHV) stainless-steel dc magnetron sputter deposition system described in detail in Ref. 5. The target was a 99.97% pure Ta disk and

sputtering was carried out in 20 mTorr (2.67 Pa) mixed Ar(99.9999%)/N₂(99.999%) discharges with N₂ fractions f_{N_2} between 0.05 and 1. Pressure was measured by a capacitance manometer and maintained constant with an automatic mass-flow controller.

Sputtering was done at a constant power of 150 W in a magnetically unbalanced mode, achieved using an external pair of Helmholtz coils.⁵ These conditions resulted in a film deposition rate of 2.34 $\mu\text{m h}^{-1}$ with $f_{\text{N}_2}=0.20$. A combination of probe,⁵ growth rate, and film composition measurements showed that the ion-to-Ta ratio incident at the substrate was 11 with an ion energy of 8 eV. Ion irradiation was essentially monoenergetic since the charge-exchange mean-free path⁶ was more than a factor of two larger than the substrate sheath width. From previous glow discharge mass spectroscopy measurements,⁷ the primary ion flux constituents are Ar⁺ (94%) and N₂⁺ (4%).

The substrates were polished 1×1×0.05 cm³ MgO(001) wafers which were cleaned as described in Ref. 8. They were then mounted on resistively heated Ta platens and inserted into the sample introduction chamber for transport into the deposition chamber. Final cleaning consisted of thermal degassing at 800 °C for 1 h, a procedure shown to result in sharp MgO(001)1×1 reflection high-energy electron diffraction patterns.⁸ The target was sputter etched for 5 min, with a shutter shielding the substrate, prior to initiating deposition. Film growth temperature, 600 °C including the contribution due to plasma heating, was measured using a pyrometer calibrated by a thermocouple bonded to a TaN-coated MgO substrate.

The microchemistry of the TaN layers was examined by Rutherford backscattering spectrometry (RBS) using 2 MeV He⁺ ions and the spectra analyzed using the RUMP simulation program.⁹ No impurities were detected. Film microstructure was investigated using a combination of XRD, plan-view TEM, and cross-sectional TEM (XTEM). XRD measurements were carried out in powder and high-resolution Philips MRD diffractometers, both with Cu K_{α} sources.

^{a)}Electronic mail: greene@mrlxp2.mrl.uiuc.edu

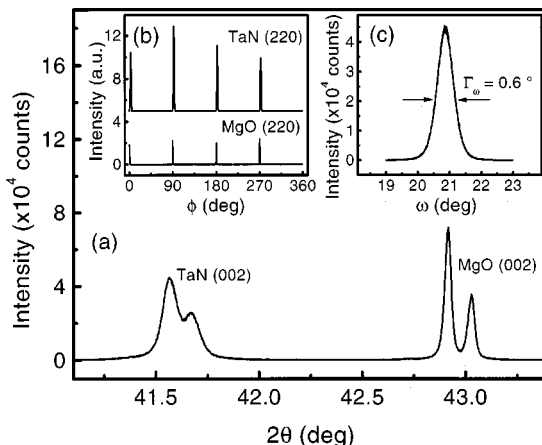


FIG. 1. XRD scans from a cubic 0.5- μm -thick TaN(001) layer grown on MgO(001) at $T_s=600^\circ\text{C}$: (a) ω - 2θ scan, (b) 220 ϕ scan, and (c) ω -rocking curve at $2\theta=41.565^\circ$.

Temperature-dependent resistivity measurements were performed using a four-point probe with evaporated Al contacts in the van der Pauw geometry. The nanoindentation responses of TaN films were determined using a Nano Indenter II instrument. Epitaxial TiN(001) layers, also grown on MgO(001) and having the same thickness as the TaN samples, served as references for calibration purposes.¹⁰ The maximum load was varied from 0.2 to 20 mN and a minimum of ten indent sequences was used for each maximum load. The triangular Berkovich diamond tip was calibrated following the procedure described in Ref. 11.

Preliminary XRD, TEM, XTEM, and RBS analyses of the microstructure and composition of as-deposited TaN_x layers were carried out as a function of f_{N_2} . As shown below, films grown with $f_{\text{N}_2}=0.20$ are single-crystal cubic TaN with a N/Ta ratio of 1.22. Decreasing f_{N_2} leads to polycrystalline layers while the use of f_{N_2} above 0.20 results in a rapid increase in resistivity leading to the appearance of N-rich second phases. We focus here on the growth of epitaxial cubic TaN.

Only one set of TaN XRD peaks was detected over the 2θ range between 20° and 80° for films grown with $f_{\text{N}_2}=0.20$. The peaks, centered at 41.57° and 41.67° and indexed as B1 NaCl structure TaN 002 $K_{\alpha 1}$ and $K_{\alpha 2}$, are shown in Fig. 1(a). The 42.92° and 43.03° peaks are due to MgO 002 $K_{\alpha 1}$ and $K_{\alpha 2}$. XRD scans along the azimuthal direction ϕ obtained in the parallel-beam mode with ω and 2θ angles optimized for the 220 peaks of MgO and TaN at a tilt angle of 45° with respect to the surface normal exhibit four 90° -rotated 220 peaks at the same ϕ angle for both MgO and TaN [Fig. 1(b)]. These results show that the film is epitaxial with a cube-on-cube relationship, $(001)_{\text{TaN}}\parallel(001)_{\text{MgO}}$ and $[100]_{\text{TaN}}\parallel[100]_{\text{MgO}}$.

The TaN lattice constant in the out-of-plane and in-plane directions determined from symmetric 002 and asymmetric 113 scans are $a_{\perp}=0.4341$ and $a_{\parallel}=0.4332$ nm. Using a Poisson ratio of 0.25 (Ref. 12), we calculate that $\approx 97\%$ of the misfit strain is relaxed during growth and obtain a relaxed lattice constant $a_0=0.4335$ nm. Previous reports for polycrystalline cubic TaN films deposited by reactive sputtering give a_0 values ranging from 0.436 to 0.442 nm (Refs. 2 and

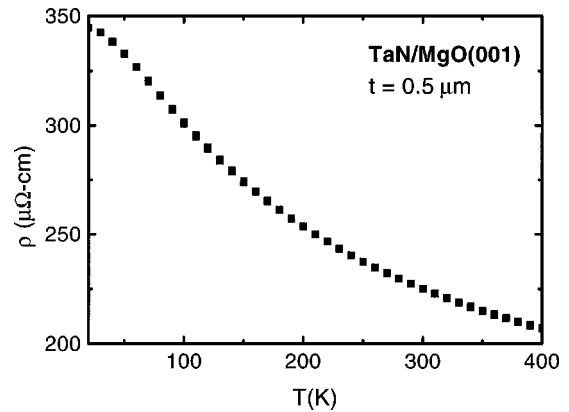


FIG. 2. Resistivity ρ of cubic TaN(001) as a function of temperature T .

13) while the lattice constant for bulk cubic TaN prepared by plasma jet heating of hexagonal TaN is 0.433 nm.¹⁴

The full width at half maximum intensity $\Gamma_{2\theta}$ of the TaN $K_{\alpha 1}$ peak is 0.10° compared to 0.04° for the MgO substrate. Figure 1(c) shows an ω -rocking curve, with $\Gamma_{\omega}=0.6^\circ$, from the TaN(001) sample corresponding to Fig. 1(a). In-plane and perpendicular x-ray coherence lengths ξ_{\parallel} and ξ_{\perp} can be obtained from the widths of the diffracted intensity distributions perpendicular Δg_{\perp} and parallel Δg_{\parallel} , respectively, to the diffraction vector \mathbf{g} using the relationships⁸ $\xi_{\parallel}=2\pi/|\Delta g_{\perp}|=\lambda/[2\Gamma_{\omega}\sin\theta]$ and $\xi_{\perp}=2\pi/|\Delta g_{\parallel}|=\lambda/[\Gamma_{2\theta}\cos\theta]$ where λ is the x-ray wavelength. From the data presented in Fig. 1, ξ_{\parallel} and ξ_{\perp} are 21 and 104 nm. The only other reported results for transition-metal nitrides were obtained for epitaxial ScN(001), $\xi_{\parallel}=15$ nm and $\xi_{\perp}=57$ nm.¹⁵ The present TaN layers exhibit higher crystalline quality with lower mosaicity.

XTEM images reveal uniform layers with abrupt film/substrate interfaces. Plan-view TEM and XTEM selected-area electron diffraction patterns are composed of symmetric single-crystal reflections whose positions are consistent with the XRD results showing cube-on-cube epitaxy.

TaN layers grown with $f_{\text{N}_2}=0.20$ were found by RBS analyses to be overstoichiometric with a N/Ta ratio of 1.22 ± 0.02 . This is analogous to the case for epitaxial TiN layers where N/Ti ratios of up to ≈ 1.2 have been reported for growth under similar conditions, relatively low homologous temperatures in the presence of ion irradiation.³ Stoichiometric TaN (N/Ta=1.0) was obtained with $f_{\text{N}_2}=0.125$; however the films, while primarily epitaxial, contained localized areas of polycrystalline growth. The stoichiometric layers had a slightly larger 001 lattice constant, $a_{\perp}=0.4356$ nm, in agreement with results for TiN and NbN in which a_0 decreases with increasing vacancy concentration on the cation sublattice. The lower strain energy associated with the growth of overstoichiometric TaN appears to stabilize pseudomorphic epitaxial growth. Further increases in N/Ta, however, result in the appearance of N-rich second phases.

The room-temperature resistivity ρ of cubic TaN layers is $225\pm 5\ \mu\Omega\text{ cm}$, independent of N/Ta ratio between 0.98 and 1.22. Previously reported values for polycrystalline cubic TaN range from 200 to $>470\ \mu\Omega\text{ cm}$.^{2,13,16,17} Figure 2 shows $\rho(T)$ for TaN(001) at temperatures from 20 to 400 K. $d\rho/dT$ is relatively small and negative, with ρ varying from

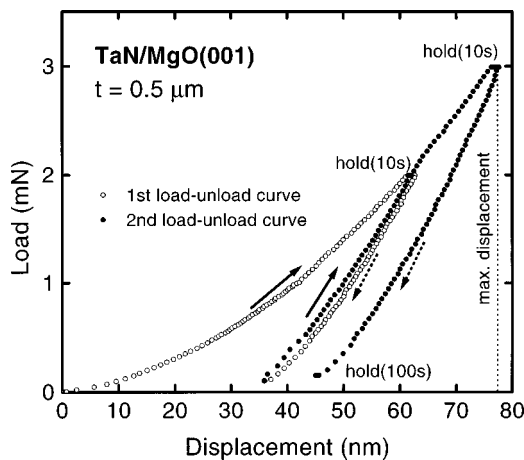


FIG. 3. Typical load-displacement curves, using maximum loads of 2 and 3 mN, obtained during nanoindentation measurements of a 0.5- μm -thick cubic TaN(001) layer grown on MgO(001) at $T_s=600^\circ\text{C}$. Hold segments are labeled and the arrows indicate the load/unload directions.

345 $\mu\Omega\text{ cm}$ at 20 K to 207 $\mu\Omega\text{ cm}$ at 400 K. In contrast to IVB-VA nitrides TiN^{3,18} and ZrN¹⁸ which show metallic behavior with positive $d\rho/dT$, VB-VA and VIB-VA alloys such as NbN_{0.97}¹⁸ and CrN¹⁹ exhibit nonmetallic resistivity with negative $d\rho/dT$.

We attribute the negative temperature coefficient of resistance for epitaxial cubic TaN_{1.22} to a weak localization of the conduction electrons, which is caused by a perturbation of the periodic crystal potential due to cation vacancies, resulting in Anderson localization.²⁰ A similar temperature dependence of the resistivity has been observed for TiO_{1.23},²¹ a compound which has the same crystal structure, number of d electrons, and cation vacancy concentration as TaN_{1.22}.

The hardness and elastic moduli of our TaN(001) layers were determined from nanoindentation measurements following the technique developed in Ref. 10. Figure 3 is a typical load-displacement curve, with 3 mN maximum load. The initial loading segment contains an elastic-plastic displacement. In order to minimize the effects of time-dependent plasticity on the measured hardness, the hold time at maximum load was 10 s for all loads. Thermal drift was calculated from a hold segment of 100 s at 95% unloading and used to automatically correct the load-displacement data through the instrument software.

The measured hardness H value for TaN(001) was found to be 30.8 ± 0.9 GPa and constant as a function of load for maximum displacements up to ≈ 80 nm, above which H decreases continuously with increasing load. This behavior is expected when the plastic zone associated with the indentation measurement penetrates through a significant fraction of the film thickness resulting in an apparent decrease in H for hard films on softer substrates, the case here where H for MgO(001) is only 9.0 ± 0.3 GPa.¹⁰ Using an estimated value

of 0.25 for the Poisson ratio ν_{TaN} ,¹² we obtain an elastic modulus E of 457 ± 16 GPa. The uncertainty in E introduced by ν_{TaN} is only 13 GPa (3%). The hardness of the metastable B1 NaCl structure TaN(001) is 54% higher than that of TiN(001) while E is nearly identical.

In conclusion, we have demonstrated the growth of epitaxial single-crystal B1 NaCl structure TaN(001). The layers have a room-temperature resistivity of 225 $\mu\Omega\text{ cm}$ with a small negative temperature dependence between 20 and 400 K. The hardness and elastic modulus, as determined by nanoindentation measurements, are 30.8 ± 0.9 and 457 ± 16 GPa, respectively.

This research was supported by the U.S. Department of Energy, Division of Materials Science, under Grant No. DEFG02-ER9645439 through the University of Illinois Frederick Seitz Materials Research Laboratory. The authors also appreciate the use of the DOE supported MRL Center for Microanalysis of Materials at the University of Illinois. C.S.S. and P.D. are partially supported by Hyundai Electronics Industries Co. (Korea) and FCAR of Québec (Canada), respectively.

- ¹N. Terao, Jpn. J. Appl. Phys. **10**, 248 (1971).
- ²D. Gerstenberg and C. J. Calbick, J. Appl. Phys. **35**, 402 (1964).
- ³J.-E. Sundgren, B.-O. Johansson, A. Rockett, S. A. Barnett, and J. E. Greene, in *Physics and Chemistry of Protective Coatings*, edited by J. E. Greene, W. D. Sproul, and J. A. Thornton (American Institute of Physics, New York, 1986), Ser. 149, p. 95.
- ⁴G. Brauer and H. Kirner, Z. Anorg. Allg. Chem. **328**, 34 (1964).
- ⁵I. Petrov, F. Adibi, J. E. Greene, W. D. Sproul, and W.-D. Münz, J. Vac. Sci. Technol. A **10**, 3283 (1992).
- ⁶A. V. Phelps, J. Phys. Chem. Ref. Data **20**, 557 (1991).
- ⁷I. Petrov, A. Myers, J. E. Greene, and J. R. Abelson, J. Vac. Sci. Technol. A **12**, 2846 (1994).
- ⁸R. C. Powell, N.-E. Lee, Y.-W. Kim, and J. E. Greene, J. Appl. Phys. **73**, 189 (1993).
- ⁹R. L. Doolittle, Nucl. Instrum. Methods Phys. Res. B **15**, 344 (1985).
- ¹⁰H. Ljungcrantz, M. Odén, L. Hultman, J. E. Greene, and J.-E. Sundgren, J. Appl. Phys. **80**, 6725 (1996).
- ¹¹W. C. Oliver and G. M. Pharr, J. Mater. Res. **7**, 1564 (1992).
- ¹²The Poisson ratio ν for TaN is not known. However, ν values for related cubic transition-metal nitrides vary only from 0.211 for TiN [J. O. Kim, J. D. Achenbach, P. B. Mirkarimi, M. Shinn, and S. A. Barnett, J. Appl. Phys. **72**, 1805 (1992)] to 0.29 for CrN [U. Wiklund, M. Bromark, M. Larsson, P. Hedenqvist, and S. Hogmark, Surf. Coat. Technol. **91**, 57 (1997)]. We used an average value of 0.25 for the calculation of a_0 and E .
- ¹³D. J. Willmott, J. Appl. Phys. **43**, 4854 (1972).
- ¹⁴JCPDS File Card No. 32-1283.
- ¹⁵D. Gall, I. Petrov, N. Hellgren, L. Hultman, J.-E. Sundgren, and J. E. Greene, J. Appl. Phys. **84**, 6034 (1998).
- ¹⁶K. Hieber, Thin Solid Films **24**, 157 (1974).
- ¹⁷B. Mehrotra and J. Stimmell, J. Vac. Sci. Technol. B **5**, 1736 (1987).
- ¹⁸L. E. Toth, *Transition Metal Carbides and Nitrides* (Academic, New York, 1971), p. 188, and references therein.
- ¹⁹I. Petrov, C.-S. Shin, D. Gall, and J. E. Greene (unpublished).
- ²⁰P. W. Anderson, Phys. Rev. **109**, 1492 (1958); N. F. Mott, Philos. Mag. **22**, 7 (1970).
- ²¹N. Tsuda, K. Nasu, A. Yanase, and K. Siratori, *Electronic Conduction in Oxides* (Springer, Berlin, 1991), p. 30.